

Spectral Appearance of Self-gravitating AGN Disks Powered by Stellar Objects: Universal Effective Temperature in the Optical Continuum and Application to Little Red Dots

YI-XIAN CHEN,¹ HANPU LIU,¹ RUANCUN LI,² BINGJIE WANG,^{1,*} YILUN MA,¹ YAN-FEI JIANG,³ JENNY GREENE,¹ ELIOT QUATAERT,¹ AND JEREMY GOODMAN¹

¹*Department of Astrophysical Sciences, Princeton University, 4 Ivy Lane, Princeton, NJ 08544, USA*

²*Max-Planck-Institut für extraterrestrische Physik, Gießenbachstraße 1, 85748 Garching bei München, Germany*

³*Center for Computational Astrophysics, Flatiron Institute, New York, NY 10010, USA*

ABSTRACT

We revisit the spectral appearance of extended self-gravitating accretion disks around supermassive black holes. Using dust-poor opacity tables, we show that all optically thick disk solutions possess a universal outer effective temperature of $T_{\text{eff}} \sim 4000 - 4500\text{K}$, closely resembling compact, high-redshift sources known as Little Red Dots (LRDs). Assuming the extended disk is primarily heated by stellar sources, this “disk Hayashi limit” fixes the dominant optical continuum temperature of the disk spectrum independent of accretion rate \dot{M} , black hole mass M_{\bullet} , and disk viscosity α , and removes the parameter-tuning required in previous disk interpretations of LRDs. We construct global self-gravitating accretion disk models with radially varying accretion rates, suggesting that burning of embedded stellar objects can both efficiently power the emission of the outer disk and hollow out the inner disk, strongly suppressing variable UV/X-ray associated with a standard quasar. The resulting disk emission is dominated by a luminous optical continuum while a separate, non-variable UV component arises from stellar populations on the nuclear to galaxy scale. We map the optimal region of parameter space for such systems and show that LRD-like appearances are guaranteed for $\dot{M}/\alpha \gtrsim 0.1M_{\odot}/\text{yr}$, a threshold insensitive to M_{\bullet} , below which the system may transition into classical non-self-gravitating AGN disks, potentially a later evolution stage. We expect this transition to be accompanied by the enhancement of metallicity and production of dust, giving rise to far infrared emission. This picture offers a physically motivated and quantitative framework connecting LRDs with AGNs and their associated nuclear stellar population.

1. INTRODUCTION

Since its launch, the James Webb Space Telescope (JWST) has uncovered a previously unrecognized class of compact, red sources known as “Little Red Dots” (LRDs; Matthee et al. 2024), which are now being identified in large numbers. These objects are unresolved in rest-optical images (e.g., Kokorev et al. 2024; Akins et al. 2025) and show broad Balmer emission lines (e.g., Greene et al. 2024; Lin et al. 2024) together with a distinctive V-shaped continuum: they are blue in the rest-frame ultraviolet (UV) but extremely red in the rest-frame optical (Labbé et al. 2023; Kocevski et al. 2024; Hviding et al. 2025), with the red optical continuum dominating the total spectral output (Greene et al. 2025). Their extreme compactness and unusual spectral energy distributions have attracted considerable attention,

motivating a range of new physical scenarios for their nature and evolution.

At first glance, the most straightforward interpretation is a conventional dust-reddened AGN accretion disk plus a stellar population component from the host galaxy (e.g. Wang et al. 2024; Labbe et al. 2024; Ma et al. 2025a; Wang et al. 2025a). However, the substantial dust extinction implied by these models is difficult to reconcile with the stringent constraints on dust emission in the rest-mid and far-infrared (FIR) from deep JWST/MIRI and ALMA observations (Williams et al. 2024; Akins et al. 2025; Casey et al. 2025; Setton et al. 2025; Wang et al. 2025a; Xiao et al. 2025). This motivates scenarios in which the optical/red bump arises from thermal emission produced by dense, gas-dominated envelopes in an almost dust-free environment. Such configurations resemble magnified versions of stellar envelopes at their Hayashi limits with a characteristic $T_{\text{eff}} \sim 5000\text{K}$ regulated by H⁻ opacity, and have been referred to as “black hole stars” or “quasi-

* NHFP Hubble Fellow

stellar”-type models (de Graaff et al. 2025a; Naidu et al. 2025; Begelman & Dexter 2025; Kido et al. 2025; Liu et al. 2025; Nandal & Loeb 2025; Wang et al. 2025c). This class of models is also motivated by strong Balmer breaks observed in a subset of LRDs (Inayoshi & Maiolino 2025; Naidu et al. 2025; Ji et al. 2025; de Graaff et al. 2025b), a feature that poses a serious challenge for both standard AGN continua and conventional post-starburst stellar populations. On the blue side, the lack of strong rest-UV continuum variability in most systems (Furtak et al. 2025; Ji et al. 2025; Zhang et al. 2025b,c) adds further tension with a conventional AGN picture and provides important additional constraints on viable physical models.

An alternative to the spherical scenario is to invoke an optically thick accretion disk (Inayoshi et al. 2025; Liu et al. 2025) as an interpretation for LRDs, in which the spectral energy distribution (SED) is obtained by integrating the thermal emission from individual disk annuli over a prescribed radial profile. The difficulty with this scenario is that, for a standard disk powered by accretion, $T_{\text{eff}} \propto R^{-3/4}$ (Shakura & Sunyaev 1973), and the spectral shape of the disk will be governed by the effective temperature at the inner boundary R_{in} . Reproducing the observed red optical continuum therefore requires imposing an inner truncation radius such that $T_{\text{eff}} \sim 5000\text{K}$, an assumption that lacks a clear physical justification from first principles.

The “inner cutoff” issue may be alleviated for extended self-gravitating disks outside the standard AGN disk’s self-gravitating radius R_{sg} , beyond which embedded stellar-objects formed from gravitational instability (GI) may replace accretion to power the disk emission and regulate the Toomre parameter $Q(R > R_{\text{sg}}) \sim 1$ (Sirko & Goodman 2003; Goodman & Tan 2004; Thompson et al. 2005; Gilbaum & Stone 2022; Chen & Lin 2024; Zhou et al. 2024; Epstein-Martin et al. 2025). For these disk regions, T_{eff} profiles can be flatter than $R^{-1/2}$ and even invert, causing the SED peak to be determined by the effective temperature at the *outer cutoff* R_{out} ¹.

This may appear to generate another issue of fine-tuning—if R_{out} were allowed to extend to arbitrarily large radii, the corresponding “dominant” T_{eff} could decline accordingly, shifting the SED peak into the far-infrared and making the spectrum too red to match those of LRDs. Indeed, Zhang et al. (2025a) apply a

constant accretion rate, self-gravitating disk model from Sirko & Goodman (2003) to fit LRD spectra and find that $T_{\text{eff}}(R_{\text{out}}) \sim 4500\text{K}$ constrains R_{out} to be no more than a factor of a few larger than R_{sg} , which also lacks a physical explanation.

In this work, we argue that $T_{\text{eff}}(R_{\text{out}})$ is not freely adjustable. Once R_{out} is defined as the outer edge of the optically thick portion of the disk capable of producing thermalized emission, the effective temperature there is set by the transition to an optically thin regime. Beyond this radius, the emission from the disk will resemble stellar populations. As long as the opacity is dust-free, consistent with the observed lack of FIR emission, the resulting T_{eff} dominating the thermalized emission is constrained to a nearly universal value. This universality intrinsically arises from the characteristic shape of the H^- opacity and can therefore be viewed as the disk analog of the Hayashi limit, directly paralleling the mechanism generating universal T_{eff} in spherical envelope models of LRDs.

One merit of these disk models is that they establish a physical connection between LRDs and standard AGNs, supported by the redshift evolution of their relative abundances (Ma et al. 2025b; Umeda et al. 2025), which implies that LRDs likely transition into AGNs after $z \sim 5$ (Inayoshi 2025). However, relevance to AGNs is a double-edged sword: another difficulty in applying the Sirko & Goodman (2003) disk model to LRDs is precisely that it connects to a standard AGN disk inside $R_{\text{sg}} \sim 1000R_g$. Zhang et al. (2025a) relies on this part of disk emission to explain the UV component of the LRDs, but the standard AGN disk picture is inconsistent with the lack of variability in the UV (e.g. Burke et al. 2025).

We propose that a more self-consistent picture is one in which the outer $Q \sim 1$ disk produces the optical/red bump, while the inner standard accretion disk is “hollowed out” (see schematic in Figure 1). Revisiting the long-standing idea that star formation in the AGN disk can deplete mass inflow, we argue that this process can naturally suppresses variable X-ray and UV radiation from the inner disk. In our picture, the observed UV emission instead arises from stellar populations in the extended optically thin cloud beyond the optically thick self-gravitating disk, which connects with nuclear stellar environments and emits stellar radiation that is *not* reprocessed into a thermal continuum. The boundary between these regions has a universal $T_{\text{eff}} \sim 4500\text{K}$, while additional emission lines may arise from both the optically thick disk and the surrounding optically thin material. Together, these elements provide a coherent explanation for the distinctive optical properties of LRDs.

¹ See also Zwick et al. (2025) where a self-gravitating disk around a supermassive star is proposed to explain the optical continuum of LRDs, although they did not explicitly model the radial profile of the disk.

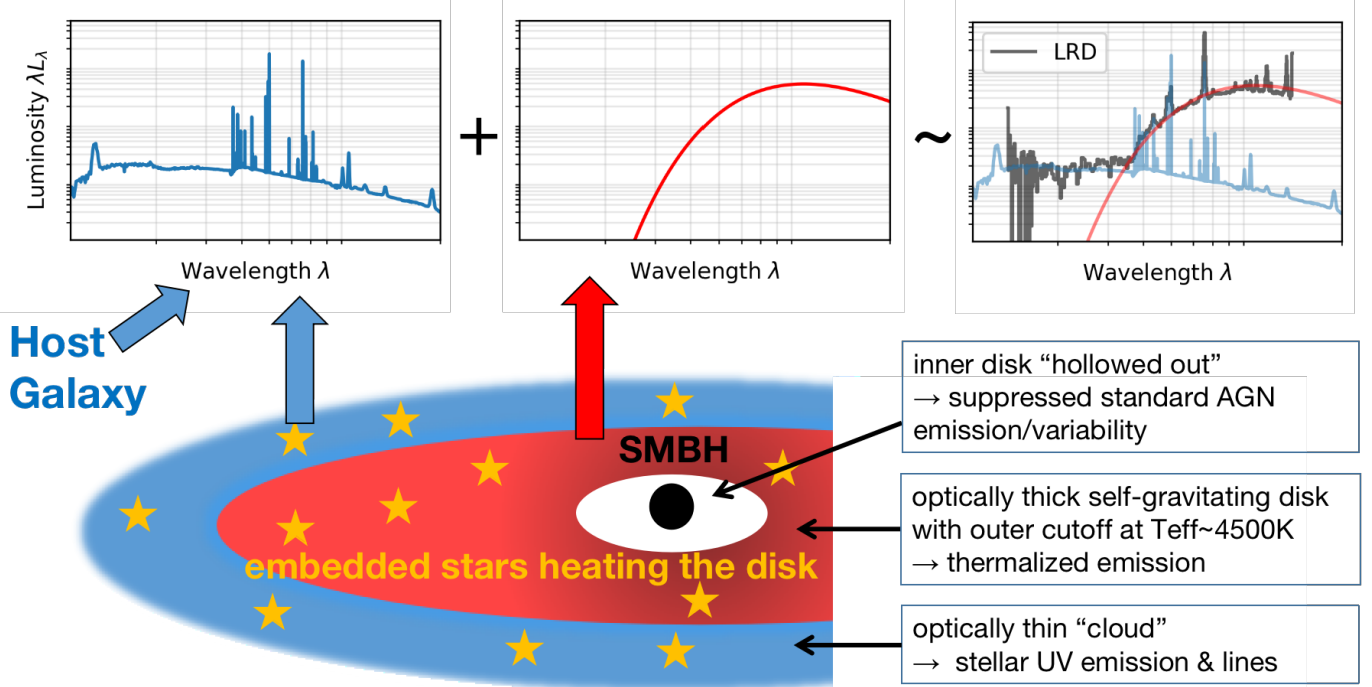


Figure 1. Schematic illustration of our proposed physical interpretation of LRDs. The dominant red/optical emission arises from an optically thick, self-gravitating disk with heating primarily supplied by embedded stellar populations. The inner disk is largely hollowed out by star formation, suppressing the classical variable UV/X-ray emission from a standard AGN. A separate UV component can originate from stellar populations in a surrounding optically thin, diffuse cloud that connects the disk to the nuclear stellar population. The top row shows a schematic spectral decomposition for illustration purpose. We use the observed spectrum of a representative LRD source RUBIES-40579 (Wang et al. 2025a) to illustrate how the total emission may be qualitatively understood as the sum of a thermalized red/optical disk component and a stellar-dominated UV component. This decomposition is not intended as a formal spectral fit, only a visual guide to the proposed physical picture.

While Thompson et al. (2005) first presented disk models with \dot{M} being depleted inwards, their application was aimed at ultraluminous infrared galaxies (ULIRGs) and employed dusty opacities, allowing R_{out} to extend to large radii and thereby producing much FIR emission. In contrast, dust-free opacity prevents R_{out} from drifting to large scales and avoids the FIR-bright regime, enabling star-forming disk models to remain consistent with the appearance of LRDs.

This paper is organized as follows: In §2 we sketch out a proof that dust-free opacity can determine a universal $T_{\text{eff}}(R_{\text{out}})$ for optically thick self-gravitating disk models, insensitive to all other assumptions. In §3 and §4, we present calculations of disk structures and demonstrate that their integrated emission is consistent with LRDs over a plausible range of parameters, and propose an evolutionary scenario in which LRDs naturally transition into standard AGNs. In §5, we compute simple disk SEDs to highlight their universal optical properties and resemblance to LRDs. Finally, in §6, we summarize our general picture and discuss future prospects in this framework for (i) modeling partially thermalized irradiation from stellar populations relevant to UV emission

and spectral lines, (ii) effect of metallicity and dust formation in the emergence of FIR emission and deviation from LRD-like appearances, (iii) implications for cosmological abundances and iv) connections to the topic of stellar-object evolution in quasar disks.

2. UNIVERSAL EFFECTIVE TEMPERATURE FOR THE BOUNDARIES OF OPTICALLY THICK DISK REGIONS

Before we solve the global radial structure of a dust-free, self-gravitating disk, we will use a local model based on a given midplane density ρ and temperature T to illustrate the universal outer T_{eff} phenomenon, regardless of the details of the radial distribution $T(R), \rho(R)$.

Using the approximate condition for marginal gravitational instability ($Q \approx 1$; Goodman 2003)

$$\Omega^2 = 2\pi G\rho \quad (1)$$

and the Eddington Equation of state

$$\rho c_s^2 = \frac{\rho \mathcal{R} T}{\mu} + \frac{a T^4}{3}, \quad (2)$$

we can write down the vertical scale height $H = c_s/\Omega$ in local parameters

$$H = \sqrt{\frac{aT^4}{6\pi G\rho^2} + \frac{\mathcal{R}T}{2\pi\mu G\rho}}, \quad (3)$$

where \mathcal{R} is the gas constant and μ is the molecular weight, taken to be 0.6 in subsequent numerical calculations. For an optically thick region, photon diffusion leads to $T^4 \approx \tau T_{\text{eff}}^4 \approx \kappa \rho H T_{\text{eff}}^4$, where σT_{eff}^4 is the flux from the photosphere of the disk.

If we take representative Rosseland mean opacity $\kappa_R(\rho, T)$ in the expression for optical depth, the effective temperatures can be expressed as a function of ρ, T

$$T_{\text{eff}} = \left[\frac{T^4}{\kappa_R(\rho, T)\rho \sqrt{\frac{aT^4}{6\pi G\rho^2} + \frac{\mathcal{R}T}{2\pi\mu G\rho}}} \right]^{1/4}, \quad (4)$$

which is self-consistent as long as $T_{\text{eff}} < T$, else the region is implied to be optically thin and the diffusion approximation will no longer be valid. This can be simplified to be

$$T_{\text{eff}} = \left[\frac{T^2}{\kappa_R(\rho, T)\sqrt{\frac{a}{6\pi G}}} \right]^{1/4} \quad (5)$$

in the radiation-pressure-dominated regime and

$$T_{\text{eff}} = T \left[\frac{2\pi\mu\rho}{\kappa_R^2(\rho, T)\mathcal{R}T} \right]^{1/8} \quad (6)$$

in the gas-pressure-dominated regime. Both will sharply decrease with temperature when $\partial \ln \kappa / \partial \ln T \gg 1$.

In Figure 2, we plot $\kappa_R(T)$ (top panel) as well as solutions of Equation 4 (lower panel) as functions of T for different values of ρ . The fiducial opacity tables (solid lines) assumes zero metallicity, such that no dust grains form at low temperatures. As a result, $\kappa_R(T)$ drops sharply and becomes extremely low at $T < 2000\text{K}$. For comparison, we also show a representative opacity and effective-temperature solution at $\rho = 10^{-12}\text{g cm}^{-3}$ using *solar-metallicity* opacity that include dust grains, plotted as green dashed curves. The opacity at different metallicities are taken from the MESA database (Paxton 2024), which is a compilation of tables from Iglesias & Rogers (1993, 1996); Ferguson et al. (2005).

The key universal feature for T_{eff} calculated from our fiducial opacity law is that regardless of ρ , most of the parameter space is consistently optically thick whereas all transition into the optically thin region must occur within the narrow parameter space where $T_{\text{eff}} \sim T \sim 4000 - 4500\text{K}$ due to the steep opacity law, suggesting

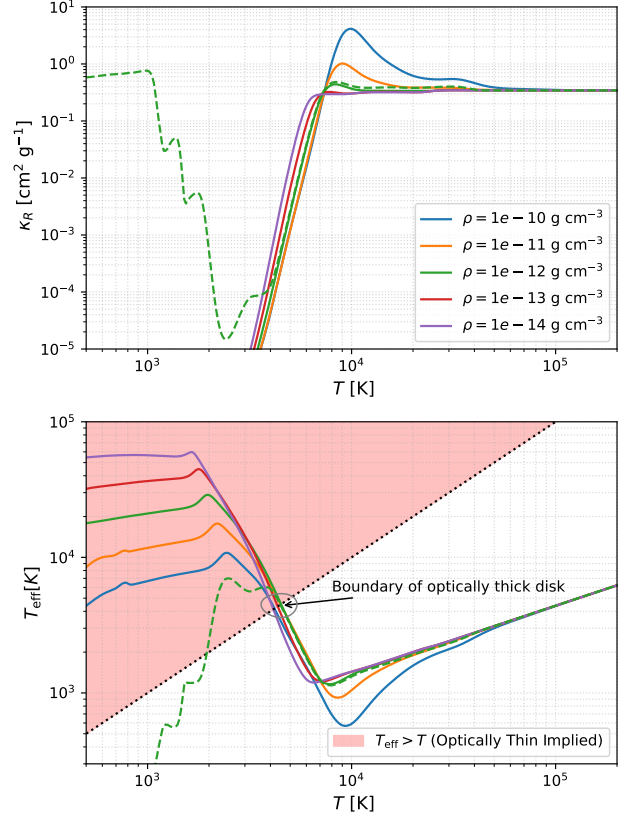


Figure 2. Top panel: solid lines indicate metal-free ($Z = 0$) Rosseland mean opacities $\kappa_R(T)$ for different densities ρ . A representative $\kappa_R(T)$ profile for solar metallicity opacity with dust for $\rho = 10^{-12}\text{g cm}^{-3}$ is shown as green dashed line for comparison. Lower panel: effective temperature calculated by Equation 4 for different densities. The shaded region represents solutions with $T_{\text{eff}} > T$ that are no longer consistent with the optically thick assumption, implying a stellar-UV rather than thermalized emission. For $Z = 0$ opacities, there is a unique and universal transition at $T_{\text{eff}} \approx T \approx 4000 - 5000\text{K}$ (gray circle), regardless of density.

a universal outer boundary T_{eff} for optically thick solutions, insensitive to the details of $\rho(R), T(R)$ and how mass flow is radially transported. This can be qualitatively taken as a self-gravitating disk version of the Hayashi limit. For high metallicity, dusty opacities (e.g. the green dashed lines), the opacity increases back up at low T and allows for an outer optically thick branch of solutions that give rise to far infrared emission at $T_{\text{eff}} < 2000\text{K}$. The dusty branch of solutions can extend to arbitrarily low midplane temperature applicable to ULIRGs (Thompson et al. 2005), but is non-existent as long as dust-free opacities is applied.

For the main calculations in this paper, we adopt the metal-free opacity (corresponding to the dust-free limit in a narrow sense) for illustrative clarity. Nevertheless,

the emergence of a universal outer effective temperature is not restricted to low metallicity, but also persists in regimes where the gas remains *broadly* dust-poor despite metal enrichment (Lee et al. 2014). This is possible if metals fail to condense into grains at low temperatures and instead remain predominantly in molecular form. The development of a possible FIR-emitting dusty branch at non-negligible grain abundance is highly relevant to connecting our LRD framework to classical AGNs, and we return to this issue in §6.2.

3. NUMERICAL SETUP FOR SOLVING DISK PROFILES

3.1. Boundary Condition

In this section, we produce simple global disk (or “ring” if the disk is hollowed out significantly) models based on three main parameters: the black hole mass M_\bullet , accretion rate at the outer boundary $\dot{M}(R_{\text{out}})$, and the disk viscosity parameter α . In order to determine R_{out} , defined as the point where $T = T_{\text{eff}}$ for given $\dot{M}(R_{\text{out}})$, we invoke a local mass accretion prescription at $Q = 1$:

$$\dot{M} = \alpha(H/R)^3 M_\bullet \Omega = \alpha(H/R)^3 M_\bullet \sqrt{GM_\bullet/R^3} \quad (7)$$

which can be inverted to obtain $H(R; \dot{M}, M_\bullet)$. We first assume Ω to be completely dominated by the potential of the supermassive black hole (SMBH), but will discuss later that this might not be the most general case. Next, we can write Equation 3 in the form of $H(R; M_\bullet, T)$ by applying the self-gravitating condition (Equation 1). With an initial guess of $T \approx 4000\text{K}$, $H(R; M_\bullet, T) = H(R; \dot{M}, M_\bullet)$ determines R_{out} and therefore $\rho(R_{\text{out}})$. The resulting T_{eff} from Equation 4 will be compared to T and iterated, such that small adjustments to T will produce a consistent solution where $T = T_{\text{eff}}$.

3.2. Integration Procedure

With the boundary condition determined by $\dot{M}, M_\bullet, \alpha$ and $R_{\text{out}}(\dot{M}, M_\bullet, \alpha)$, we solve the self-gravitating disk with a procedure similar to Thompson et al. (2005); Chen & Lin (2024). At any radius R for given M_\bullet , the density ρ is determined by the self-gravitating condition. The mass transport equations will yield $H(R; \dot{M}, M_\bullet)$, which can be substituted into Equation 3 to solve for T given density ρ . The combination (ρ, T) is then substituted into Equation 4 to calculate T_{eff} , using the metal-free opacity tables. The key qualitative difference from Sirko & Goodman (2003) is that we relax the assumption of constant \dot{M} to become a general self-similar profile in the $Q \sim 1$ region to account for depletion of gas by formation and growth of embedded stellar objects:

$$\dot{M}(R) = \dot{M}(R_{\text{out}})(R/R_{\text{out}})^\gamma \quad (8)$$

which closes the equation set for disk profiles $\dot{M}(R), H(R), T(R), \rho(R), T_{\text{eff}}(R)$. For demonstration, we provide in the Appendix analytical self-gravitating disk profiles for $\rho(R), T(R)$ in the radiation pressure dominated limit, which are most relevant to our results, as well as the corresponding $T_{\text{eff}}(R)$ assuming power law opacities, which shows that self-gravitating disks generally exhibit flat or even inverted $T_{\text{eff}}(R)$ profiles. As a result, the SED of such disks will be dominated by emission from R_{out} .

The self-gravitating disk stops at an inner radius where viscous heating is sufficient to power the disk emission

$$\frac{3G\dot{M}(R_{\text{sg}})M_\bullet}{4\pi R_{\text{sg}}^3} = 2\sigma T_{\text{eff}}^4(R_{\text{sg}}), \quad (9)$$

and within R_{sg} the disk should connect to a standard disk (where we expect no star formation to further reduce the mass inflow) with a constant $\dot{M}(R_{\text{sg}})$ and an integrated luminosity of $\sim \epsilon_\bullet \dot{M}(R_{\text{sg}})c^2$ in the UV/X-ray, with the radiative efficiency ϵ_\bullet determined by the standard AGN inner cutoff close to a few gravitational radii R_g . In our picture of LRDs, this emission should be dominated by outer stellar emission regardless of the inner disk structure (e.g. see Figure 8). But for completeness, we do solve a standard disk structure within R_{sg} using the viscous disk equations (Shakura & Sunyaev 1973) assuming a constant accretion rate.

When $\gamma = 0$, the disk profile is qualitatively similar to the constant- \dot{M} solutions in Sirko & Goodman (2003) (although we specifically use a different metal-free opacity). When $\gamma > 0$, the profile may be linked with an effective energy conversion rate at each radius as

$$\frac{d\dot{M}}{dR} = \gamma(\dot{M}(R_b)/R_b)(R/R_b)^{\gamma-1} = 4\pi \frac{\sigma T_{\text{eff}}^4}{\epsilon c^2} R. \quad (10)$$

Note that the physical value of ϵ can vary widely from $\sim 10^{-4} - 10^{-3}$ for a stellar population (Thompson et al. 2005; Tagawa et al. 2020), to $\sim 10^{-2}$ for massive stars, and up to ~ 0.1 for stellar-mass black holes (Gilbaum & Stone 2022; Epstein-Martin et al. 2025). In addition, stellar winds and outflows may reduce the effective ϵ by removing mass from the system without contributing significant heating. Given these large uncertainties, rather than assuming a fixed ϵ , we adopt a flexible power-law form for $\dot{M}(R)$. A fixed ϵ could in fact lead to local and/or global (radial) instabilities that drive $\dot{M}(R)$ toward a self-regulated power-law behavior. We therefore interpret $\epsilon(R)$ as an effective, radius-

dependent conversion efficiency, whose detailed implications will be discussed later.

4. RESULTS

4.1. Fiducial Models at $M_\bullet = 10^6 M_\odot$ and Implied Constraints

In Figure 3 we present fiducial models with $M_\bullet = 10^6 M_\odot$, $\alpha = 0.1$ and outer boundary accretion rates of $\dot{M} = 0.1 M_\odot/\text{year}$ (opaque lines) and $\dot{M} = 1 M_\odot/\text{year}$ (semi-transparent lines). The self-consistently determined outer boundary, no longer a free parameter of the models, are calculated by the method described in §3.1. At a small decay slope $\gamma \sim 0.1$ (blue lines), we obtain classical solutions similar to the optically thick, self-gravitating region of the [Sirk & Goodman \(2003\)](#) disk model where mass removal is modest, and the local transport equation yields $H \propto R^{3/2}$ and $c_s = \text{Const}$. For radiation pressure dominated regions, the midplane temperature decreases with R (or increases inwards), and the disk extends to $R_{\text{sg}} \sim 0.2 R_{\text{out}}$ (indicated by vertical dotted lines) before it transitions into an inner α -disk. Between R_{sg} and R_{out} , we expect the disk emission to be dominated by the effective temperature close to the outer boundary due to an increasing $T_{\text{eff}}(R)$, with cooler annuli contributing to a long-wavelength tail in the SED (see §5 for representative spectral distributions).

However, before detailed spectral modeling, we can anticipate that if most of the accreting material is efficiently transported inward, a mass accretion rate of $\dot{M}(R_{\text{sg}}) \approx \dot{M}(R_{\text{out}})$, will feed the inner region $R < R_{\text{sg}}$. This inner zone, powered solely by viscous dissipation, will radiate like a standard thin AGN disk, producing a UV-bright component with luminosity

$$L_{\text{AGN}} = \epsilon_\bullet \dot{M}(R_{\text{sg}}) c^2 = 3.4 \times 10^{44} \left(\frac{\epsilon_\bullet}{0.06} \right) \left(\frac{\dot{M}(R_{\text{sg}})}{0.1 M_\odot/\text{yr}} \right) \text{erg/s}, \quad (11)$$

so unless an additional inner truncation $\gg R_g$ suppresses the radiative efficiency ϵ_\bullet ([Liu et al. 2025](#)), L_{AGN} from the inner disk would produce strongly variable UV and potentially also X-ray emission incompatible with LRDs. To avoid this, we favor models with larger decay slope γ , where a large fraction of the inflowing mass is lost or converted into stars, reducing the amount that reaches the inner disk and robustly suppressing standard AGN features. For instance, at $\gamma = 0.4$ (orange lines in Figure 3), only about half of $\dot{M}(R_{\text{out}})$ is able to penetrate inward to power the inner disk for both accretion rates, and the transmitted fraction further reduces for higher γ , making the inner disk less and less luminous.

Eventually at sufficiently large γ , a qualitative transition occurs: the disk reaches an optically thin branch before the self-gravitating radius, at a radius $R_{\text{thin}} > R_{\text{sg}}$. This behavior is evident in the $\gamma = 0.8$ case for $\dot{M} = 0.1 M_\odot/\text{yr}$ in Figure 3 (green opaque lines). This is due to the strong depletion of \dot{M} that yields $\partial T(R)/\partial R > 0$ within a certain radius and makes T_{eff} and T converge inwards. When this happens, we terminate the iterative solution at R_{thin} . We do not attempt to model the detailed physics in this optically thin region which is uncertain, same as the reason we do not model the optically thin cloud exterior to R_{out} .

Regardless of what additional star formation might occur inside R_{thin} , any remaining accretion that does reach the viscous inner disk would produce, at most, an AGN luminosity of

$$L_{\text{AGN,max}} = \epsilon_\bullet \dot{M}(R_{\text{thin}}) c^2 \quad (12)$$

where the actual AGN luminosity can be between 0 and $L_{\text{AGN,max}}$, depending on how much accretion rate is converted to stars within the region $< R_{\text{thin}}$. In practice, for radiation pressure dominated disks, in the presence of R_{thin} which only occurs at high γ , the luminosity of the outer, optically thick disk or “ring” will typically exceed that of the inner components even if the residual accretion were fully converted into standard disk UV emission.

In all cases, the implied $\epsilon(R)$ has a very large range between $\sim 10^{-4}$ to ~ 1 in the self-gravitating region (lower right panel of Figure 3), implying that global regulation processes need to be at work to maintain a self-similar \dot{M} profile, rather than the burning of specific population of stars at isolated regions.

To more quantitatively demonstrate the decrease of the inner disk’s emission with γ , in Figure 4 we plot L_{AGN} or $L_{\text{AGN,max}}$ (as upper limits at sufficiently high γ), as well as the thermal emission of the optically thick self-gravitating disk region L_{disk} for comparison, defined to exclude contributions from the standard inner disk and any optically thin zones, keeping in mind they do not contribute to the red/optical continuum that we are interested in:

$$L_{\text{disk}} = 2\pi \int_{R_{\text{thin}} \text{ or } R_{\text{sg}}}^{R_b} 2\sigma T_{\text{eff}}^4 R' dR', \quad (13)$$

as a function of γ for a variety of \dot{M} and α , including the two cases shown in Figure 3. The trend clearly demonstrates that in all cases, as γ increases, the standard-AGN luminosity declines while the outer-disk emission dominates. For $\dot{M} \gtrsim 1 M_\odot/\text{yr}$, the inner disk emission dominates over L_{disk} at $\gamma = 0$, requiring

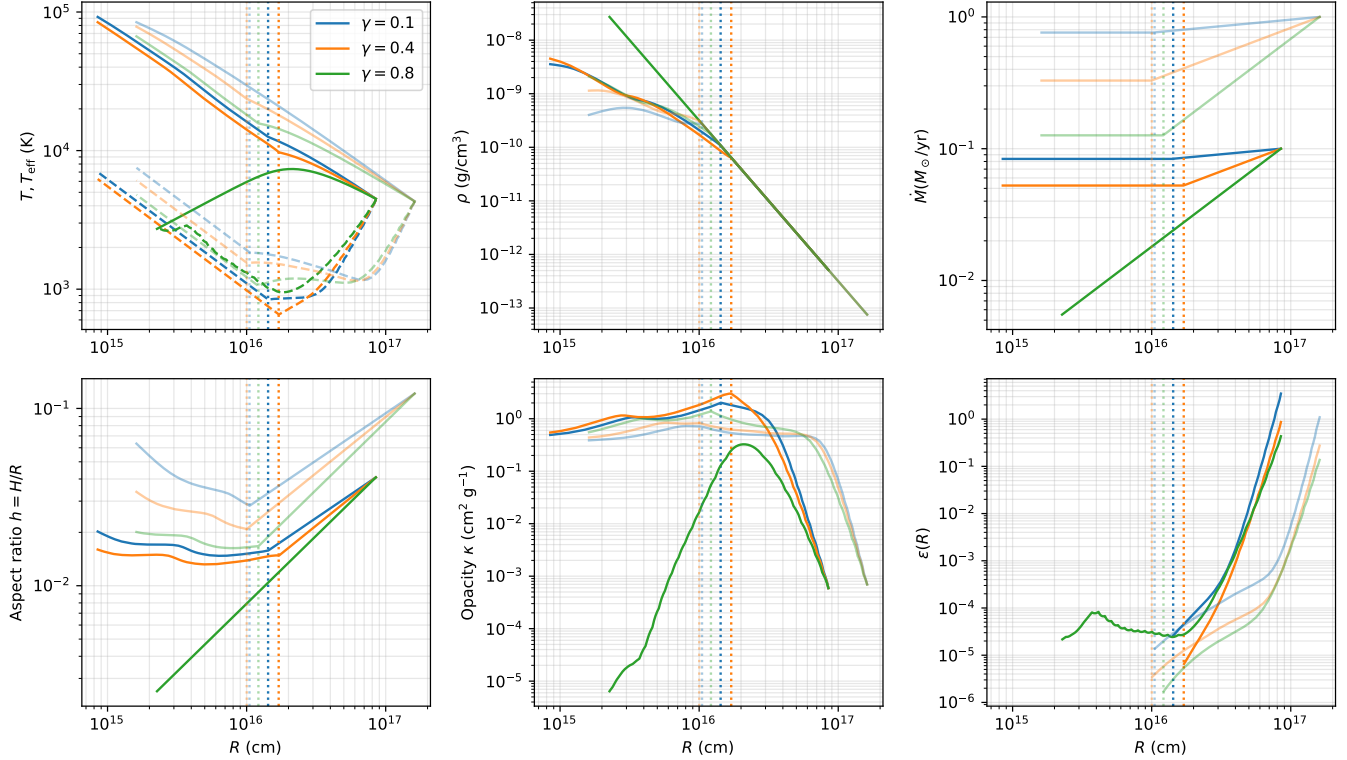


Figure 3. Radial structure of fiducial disk solutions for $M_\bullet = 10^6 M_\odot$, $\alpha = 0.1$ and outer boundary accretion rates of $\dot{M} = 0.1 M_\odot/\text{year}$ (opaque lines) and $\dot{M} = 1 M_\odot/\text{year}$ (semi-transparent lines), with varying mass-loss slope γ . The midplane temperature T and effective temperature T_{eff} are shown in solid and dashed lines respectively in the top left panel. The transition towards an inner viscous α -disk, if present, is indicated by vertical dotted lines.

a significant γ to reduce the standard-AGN UV and X-ray component and be consistent with the appearance of LRDs.

Orthogonal to the constraint on γ set by L_{AGN} , let us now discuss constraints on more intrinsic parameters such as $M_\bullet, \dot{M}, \alpha$. It may not be particularly surprising that L_{disk} is nearly independent of γ in all cases since it is dominated by the emission at the outermost radius

$$L_{\text{disk}} \approx 2\pi f R_{\text{out}}^2 \sigma T_{\text{eff}}(R_{\text{out}})^4, \quad (14)$$

where f is a numerical factor taking into account the effective width of the annuli radiating at $T_{\text{eff}}(R_{\text{out}})$, $\Delta R \sim f R_{\text{out}}$. Since the $T_{\text{eff}} - R$ power law is insensitive to γ (see Appendix), f is quite universal and for each $M_\bullet, \dot{M}, \alpha$ parameter input, L_{disk} is well determined by the disk profile close to R_{out} . Making use of Equation 3 and Equation 7, we can write R_{out} in the radiation pressure dominated scenario as

$$R_{\text{out}} = \left[\frac{GM_\bullet^{3/2}\dot{M}(R_{\text{out}})}{\alpha} \left(\frac{3}{2\pi a T_{\text{eff}}^4(R_{\text{out}})} \right)^{3/2} \right]^{2/9}, \quad (15)$$

technically an implicit relation. However, for universal $T_{\text{eff}}(R_{\text{out}}) \approx 4000\text{K}$, we can write (hereon we use \dot{M} to represent the accretion rate at the outer boundary)

$$R_{\text{out}} \approx 0.03\text{pc} \left(\frac{\dot{M}/\alpha}{1M_\odot\text{yr}^{-1}} \right)^{2/9} \left(\frac{M_\bullet}{10^6 M_\odot} \right)^{1/3} \left(\frac{T_{\text{eff}}}{4000\text{K}} \right)^{-3/4} \quad (16)$$

which gives a fair approximation of our numerical outcomes, and correspondingly,

$$\begin{aligned} L_{\text{disk}} &\approx 2 \times 10^{44} \text{ergs}^{-1} \left(\frac{f}{0.25} \right) \left(\frac{\dot{M}/\alpha}{1M_\odot\text{yr}^{-1}} \right)^{4/9} \\ &\times \left(\frac{M_\bullet}{10^6 M_\odot} \right)^{2/3} \left(\frac{T_{\text{eff}}}{4000 \text{ K}} \right)^{5/2} \\ &= 2L_{\text{Edd}}(M_\bullet) \left(\frac{f}{0.25} \right) \left(\frac{\dot{M}/\alpha}{1M_\odot\text{yr}^{-1}} \right)^{4/9} \\ &\times \left(\frac{M_\bullet}{10^6 M_\odot} \right)^{-1/3} \left(\frac{T_{\text{eff}}}{4000 \text{ K}} \right)^{5/2}. \end{aligned} \quad (17)$$

This explains why in Figure 4 the self-gravitating disk's luminosity is nearly the same for $\alpha = 0.1, \dot{M} =$

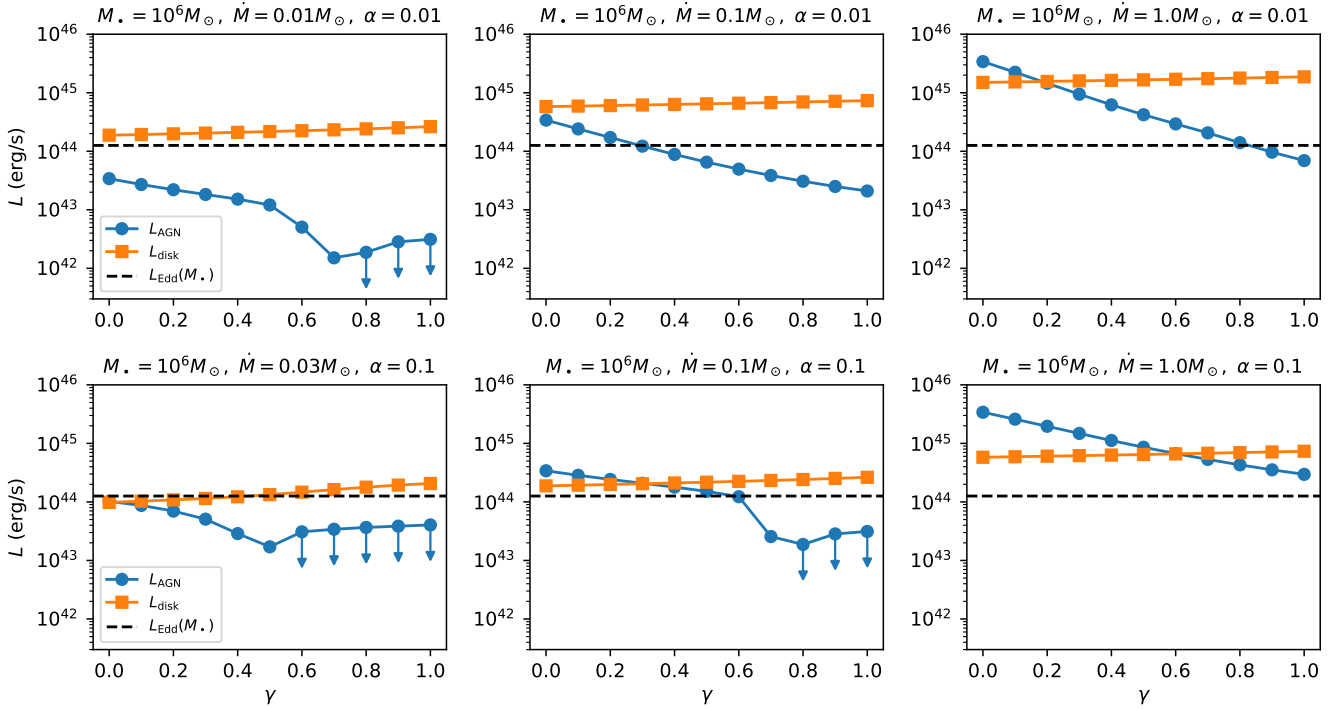


Figure 4. Summary of luminosity contributions for the accretion disk around a $10^6 M_\odot$ SMBH. The AGN component or its upper limit is shown in blue and the thermal emission from the optically thick self-gravitating region is shown in orange. The Eddington luminosity is plotted for reference (black dashed). Across all models, increasing γ systematically suppresses L_{AGN} , while L_{disk} remains largely unchanged and often dominates even at γ for lower accretion rates.

$0.1 M_\odot/\text{year}$ and $\alpha = 0.01$, $\dot{M} = 0.01 M_\odot/\text{year}$ since both R_{out} and L_{disk} are only sensitive to their ratio and increases with \dot{M}/α . The numerical factor $f \approx 0.25$ is calibrated on our obtained L_{disk} values. When \dot{M}/α is too large, L_{disk} becomes significantly higher than the Eddington luminosity of the SMBH (dashed horizontal lines). This has the consequence of requiring a total luminous mass $> M_\bullet$ (e.g. massive stars, stellar-mass BHs at their Eddington luminosity) in the outer disk as heat source to support L_{disk} . The radiation field of embedded stars may be anisotropic to allow for super-Eddington luminosity in polar solid angles (Chen et al. 2025c), but this can only relax the threshold by order of a few. Eventually, as $L_{\text{disk}} \gg L_{\text{Edd}}$, assuming Ω to be dominated solely by the SMBH's gravitational potential will no longer be self-consistent. Thus, the current framework is fully applicable only for moderate values of \dot{M}/α . This limitation is not a physical prohibition; rather, it implies that modeling systems with very large \dot{M}/α requires a more complete and dynamical treatment that self-consistently follows the transition from massive star-dominated to a SMBH-dominated potential with a general $\Omega(r)$ profile, which we will address in future works. As we will elaborate later in this section, such a regime likely corresponds to the earliest phases of LRD

evolution, where \dot{M} is high and starburst is extremely rapid. As the accretion rate declines and/or angular-momentum transport becomes more efficient, the total stellar mass may be self-regulated towards moderate levels. We take this transition limit for $L_{\text{disk}} \leq 3L_{\text{Edd}}$ as

$$\dot{M}/\alpha < 3 M_\odot \text{yr}^{-1} \left(\frac{T_{\text{eff}}}{4000 \text{ K}} \right)^{-45/8} \left(\frac{M_\bullet}{10^6 M_\odot} \right)^{3/4} \left(\frac{f}{0.25} \right)^{-9/4} \quad (18)$$

For LRD-like appearance, another physical limit on \dot{M}/α arises from the requirement that a substantial portion of the disk must remain self-gravitating. This is guaranteed for radiation pressure dominated disks: combining Equation 16 with the viscous support condition (Equation 9), a radiation pressure dominated disk would not be viscously supported at R_{out} for any accretion rates lower than $\sim c^3/G$, an unphysically enormous rate. Practically, we find that the disk would become marginally viscously supported close to R_{out} only if gas pressure were to dominate immediately within R_{out} , a premise that can be avoided as long as

$$\rho(R_{\text{out}}) = \frac{M_\bullet}{2\pi R_{\text{out}}^3} < 1.2 \times 10^{-12} \text{ g/cm}^3 \left(\frac{T_{\text{eff}}}{4000 \text{ K}} \right)^3 \quad (19)$$

such that the material is radiation dominated at $T \approx T_{\text{eff}} \approx 4000\text{K}$. This requires

$$\dot{M}/\alpha > 0.1 M_{\odot}\text{yr}^{-1} \left(\frac{T_{\text{eff}}}{4000 \text{ K}} \right)^{-9/8} \quad (20)$$

independent of the SMBH mass. Below this threshold, the disk may behave as a classical AGN, possibly representing the late evolutionary stages of LRDs (Fu et al. 2025). It is worth noting that the global angular-momentum transport mechanism proposed by Thompson et al. (2005), in which the inflow velocity scales as

$$v_r \sim m(H/R)\Omega R \gg \alpha(H/R)^2\Omega R \quad (21)$$

has an effect qualitatively similar to adopting a large effective α . In their model, this enhanced transport is invoked specifically to *prevent* mass being converted into stars too efficiently in the self-gravitating region and to maintain sustained fueling of the AGN, corresponding to the low \dot{M}/α parameter space. In contrast, our emphasis is on the regime where angular-momentum transport is *inefficient*, causing the AGN to be underfed and the inner disk to be hollowed out, producing LRD-like appearances.

4.2. Dependence on SMBH masses

Previous calculations offer us some anticipation of the dependencies of R_{out} , L_{disk} and relevant constraints on M_{\bullet} , and in this subsection we verify those with numerical results for other SMBH masses.

Figure 5 shows an example of the $\alpha = 0.1$ profiles for $10^7 M_{\odot}$ at outer-boundary accretion rates of $\dot{M} = 0.1 M_{\odot}/\text{year}$ (opaque lines) and $\dot{M} = 1 M_{\odot}/\text{year}$ (semi-transparent lines). Compared to Figure 3, apart from having larger R_{out} (as expected from Equation 16) which implies a larger total disk luminosity, and scaled-up h and ϵ values, the rest of the profiles ρ, T, T_{eff} are similar to Figure 3 both in the self-gravitating regime and in the viscous α -disk, regardless of the specific M_{\bullet} or R values due to the self-similarity of the equations (e.g. see Appendix).

Figure 6 compares the luminosity components for several choices of \dot{M} and α given a $M_{\bullet} = 10^7 M_{\odot}$ or $10^5 M_{\odot}$ SMBH. At given \dot{M}/α , $L_{\text{disk}}/L_{\text{Edd}}$ scales down with SMBH mass consistent with Equation 17, and the system is more likely to enter the stellar-potential dominated limit at lower M_{\bullet} (18).

We now more generally illustrate the constraints from Equations 18 and 20 in Figure 7. The white region delineates the parameter space in which our results most robustly apply, namely LRD systems with gravity dominated by the SMBH potential. Within the red region,

sustaining L_{disk} would require the mass of luminous stellar sources to exceed M_{\bullet} . The dynamical structure of such systems would instead be governed by the stellar potential, leading to a flatter angular-frequency profile $\Omega(R)$ profile than the Keplerian case. Nevertheless, the argument in §2 does not hinge on particular rotation profiles so we still expect LRD-like optical continuum properties.

At the opposite extreme, the lower bound on \dot{M}/α is a limit beyond which the system transitions into a standard, nonself-gravitating AGN disk (gray region). The white region narrows toward lower M_{\bullet} , with the two boundaries approaching each other for $M_{\bullet} \lesssim 10^4 M_{\odot}$.

Taken together, the three regimes likely represent successive phases of the coupled LRD-AGN evolution. We envisage that a finite gas reservoir suddenly starts to fuel the SMBH from large radii. During the earliest stage, when the disk experiences strong external infall, angular momentum transport from turbulence is weak in radiation-pressure-dominated environments (Jiang & Goodman 2011; Chen et al. 2023b), preventing efficient inflow and leaving the AGN dormant while accretion flows are converted into rapid starbursts in the outer regions.

With the presence of a large stellar population, non-axisymmetric stellar bars and spirals may facilitate angular momentum transport (leading to larger effective α or m) (Goodman & Rafikov 2001; Hopkins & Quataert 2010)². During this phase, the SMBH itself may grow not only through accretion from a thin disk but also via the engulfment of stellar material. Together with a declining mass supply \dot{M} , these processes drive the system toward a regime of moderate \dot{M}/α larger M_{\bullet} , in which the SMBH potential dominates the gravity of LRDs.

At later times, the depletion of external gas fuel leads to a further decline of \dot{M} , quenching gravitational instability, and the system enters the classical quasar phase. Additionally, chemical enrichment from stellar evolution (Cantiello et al. 2021; Ali-Dib & Lin 2023; Xu et al. 2025) can gradually introduce metallicity and dust, giving rise to FIR emission as we discussed in §2 and will revisit in §6.2. By this stage, the system can naturally evolve into classical quasars in multiple aspects (higher M_{\bullet} , standard disk and dust emission), completing the evolutionary cycle.

5. EXAMPLE SPECTRAL APPEARANCES

As described in §2, all our optically thick disk models naturally yield characteristic $T_{\text{eff}} \approx 4500\text{K}$ at their outer

² Rozyczka et al. (1995) also showed that supernova occurring in quasar disks can enhance angular momentum transport.

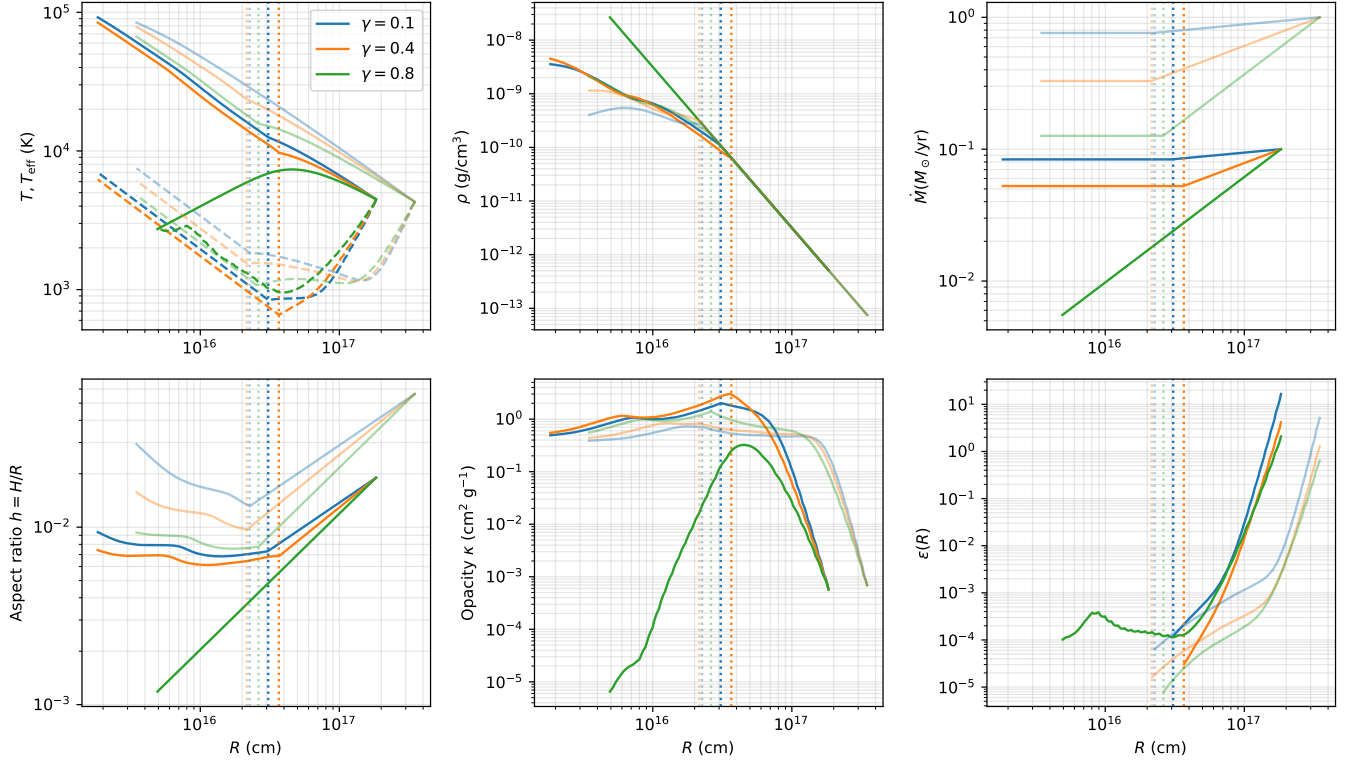


Figure 5. Radial structure of fiducial disk solutions for $M_* = 10^7 M_\odot$, $\alpha = 0.1$ and outer boundary accretion rates of $\dot{M} = 0.1 M_\odot/\text{year}$ (opaque lines) and $\dot{M} = 1 M_\odot/\text{year}$ (semi-transparent lines), similar to Figure 3.

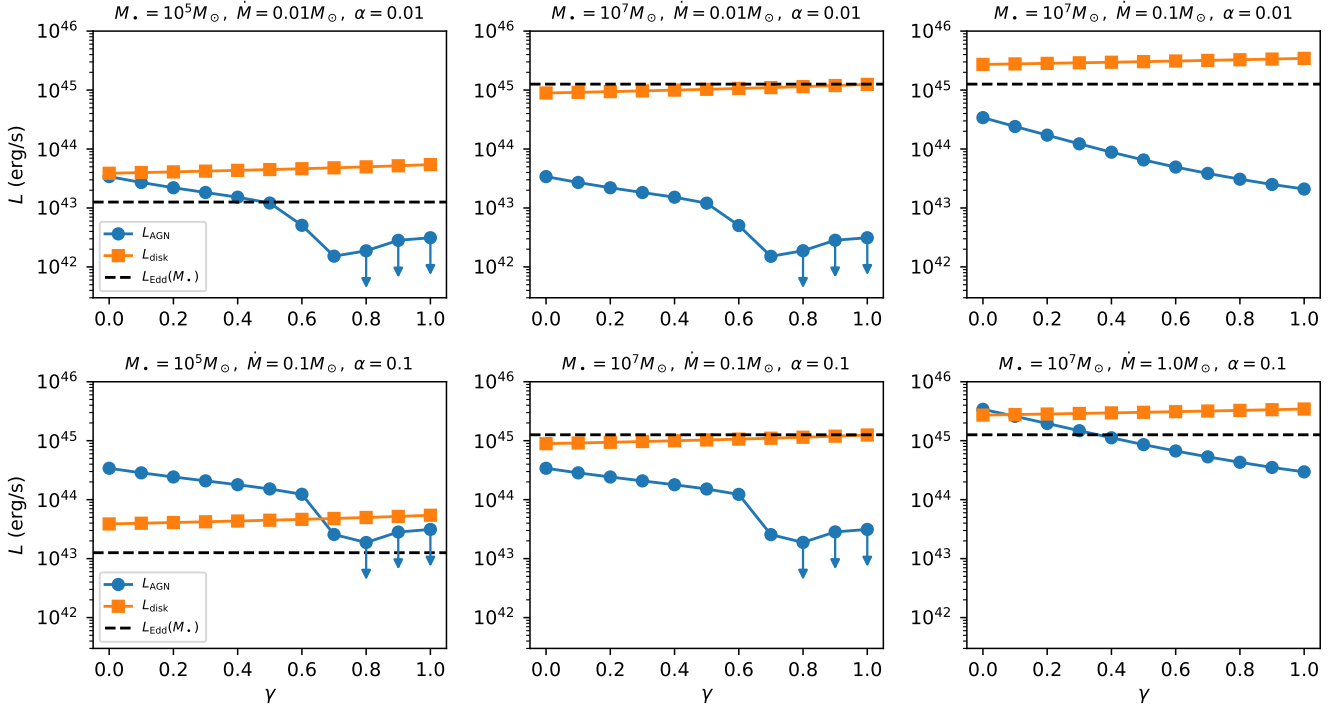


Figure 6. Summary of luminosity contributions for the accretion disk around a $10^7 M_\odot$ or $10^5 M_\odot$ SMBH for certain accretion rates and α .

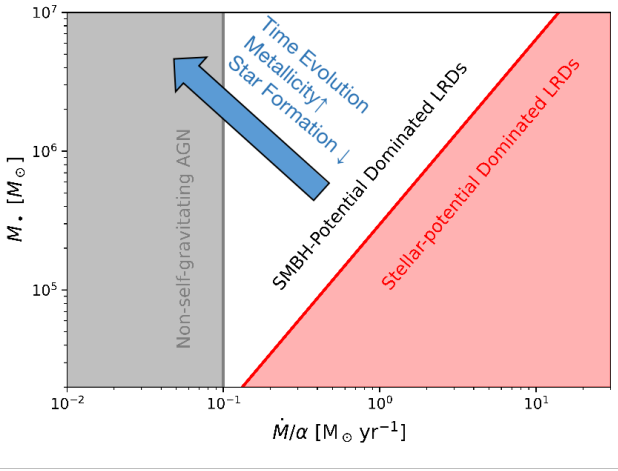


Figure 7. Parameter space of SMBH accretion disk in the $(\dot{M}/\alpha, \dot{M})$ plane. Red indicate regime of dynamical starburst where luminous mass $> M_\bullet$ is needed to support L_{disk} (Equation 18), while the gray region marks the transition to a nonself-gravitating AGN disk (Equation 20). These regimes may reflect sequential stages of SMBH disk evolution, transitioning from LRD-like systems to standard AGN disks.

truncation radii. This temperature regulation ensures that the disks robustly produce a red optical component similar to LRDs without requiring additional parameter tuning. To emphasize this point, we compute the full spectral energy distributions (SEDs) by integrating the thermal emission over all disk annuli from R_{out} to i) $10R_g$ of the SMBH if a standard α -disk is present or ii) to R_{thin} if otherwise. The observed spectrum of a representative LRD, RUBIES-40579 (Wang et al. 2025a), is shown in the background for comparison, illustrating the similarity between the predicted red/optical bump and the observed LRD SED. The left panel of Figure 8 presents the SEDs for representative disk models spanning a range of (M_\bullet, \dot{M}) at fixed $\alpha = 0.01$. The solid curves correspond to models with $\gamma = 1$ and demonstrate the universal red/optical bump across different parameter choices. The dashed and dotted curves have $\gamma = 0.5$ and $\gamma = 0.1$, respectively, for a given parameter $M_\bullet = 10^7 M_\odot, \dot{M} = 0.01 M_\odot/\text{yr}$, illustrating how the inner disk’s UV emission progressively weakens as γ increases. The right panel shows the corresponding outer disk luminosities, L_{disk} , plotted against the effective temperature at the outer radius, which sets the peak of the red/optical emission and illustrates the emergence of a “Hayashi-limit” for self-gravitating disks across 2-3 order of magnitudes in luminosity. Hollow circles indicate a factor of ~ 0.1 reduction in the inferred luminosity, representative of plausible viewing angle effects due to $H/R \sim 0.1$. We also comment that such optical/red bumps, if fitted as a modified blackbody $F_\nu \propto B_\nu(T)\nu^\beta$,

will most likely prefer a broader $\beta \leq 0$ due to the initial decay of $T_{\text{eff}}(R)$ inwards down to $1000 - 2000\text{K}$, consistent with a considerable number of samples in de Graaff et al. (2025a). This is also consistent with LRD samples presented in Wang et al. (2026), whose emission contain contribution from $T_{\text{eff}} \lesssim 3000\text{K}$ atmosphere components with water absorption features. Nevertheless, we caution that the exact shape of the thermal emission depends on radiative transfer effects and may deviate from a blackbody (H. Liu et al., in prep), and detailed fitting will not be the focus of this paper.

6. SUMMARY AND DISCUSSION

We have developed a framework in which the blackbody-like, dominant optical emission of LRDs arise from optically thick, dust-poor, self-gravitating disks regulated by an outer boundary T_{eff} set by the H^- opacity. This “disk Hayashi limit” fixes the characteristic optical continuum temperature at $T_{\text{eff}} \sim 4500\text{K}$ largely independent of black-hole mass, accretion rate, or turbulent viscosity. Furthermore, allowing for radially declining accretion rates due to star formation and feedback naturally suppresses the inner standard AGN disk, yielding spectra dominated by a thermalized optical bump while remaining consistent with the weak variability and lack of strong X-ray emission observed in LRDs.

In a time-dependent picture, these systems can be interpreted as an evolutionary phase towards later classical quasars. During the earliest stages, strong inflow and inefficient angular-momentum transport favor rapid formation of stars in a self-gravitating disk, whose potential could dominate over the SMBH potential. As the SMBH grows, the external gas supply declines and the stellar potential’s non-axisymmetric structures provide angular-momentum transport (Hopkins & Quataert 2010), the total stellar mass required to power the disk is regulated and SMBH potential dominates gravity. At still later times, continued depletion of external gas supply and increasing metallicity allow the disk to lose its LRD-like characteristics and evolve into a standard AGN disk.

Finally, in this section, we discuss several directions for future work within this framework, including the role of stellar irradiation in producing the UV continuum and emission lines, the impact of metallicity and dust formation on the emergence of FIR-emission and transition to classical AGNs, cosmological abundance implications, and the connection to studies on stellar evolution in AGN disks.

6.1. UV continuum and Broad Emission Lines

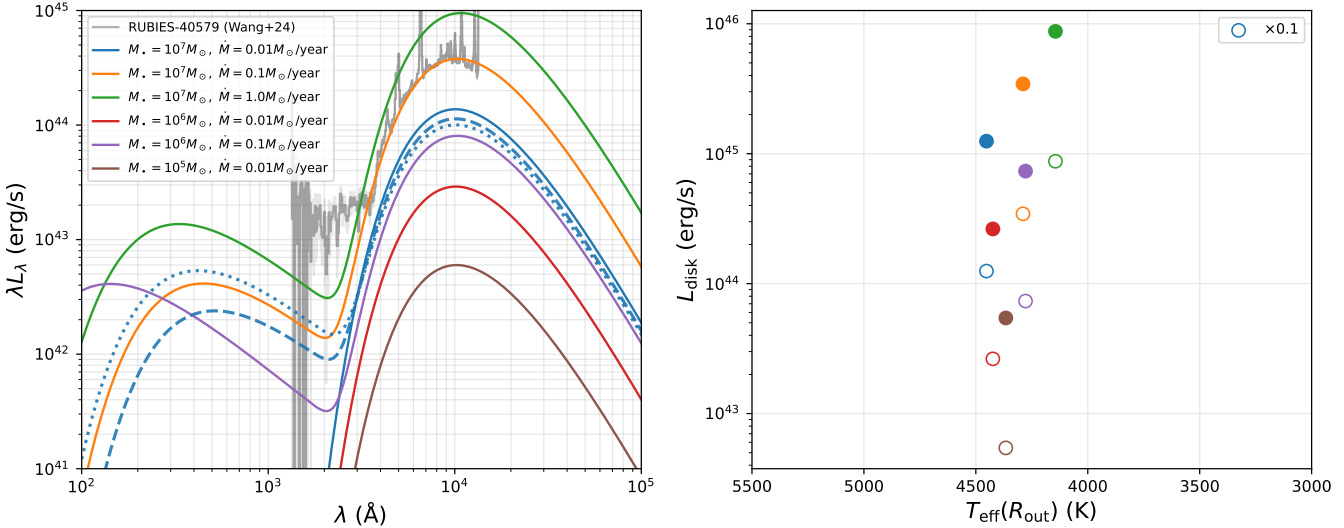


Figure 8. Left: Example SEDs for selected $\alpha = 0.01$ disk models by integrating blackbody emission over each disk annuli. All solid lines assume $\gamma = 1$ while the dashed and dotted lines correspond to M_* = $10^7 M_\odot$, \dot{M} = $0.01 M_\odot/\text{yr}$ model with $\gamma = 0.5, 0.1$ respectively which allows for more UV radiation from the inner AGN disk. We vary \dot{M}, M_* and not α since we expect from Equation 17 that disks with similar \dot{M}/α at given M_* will have similar emission and so they can be scaled to higher viable α values easily. A representative LRD spectrum (RUBIES-UDS 40579) is plotted in gray. Right: disk luminosity versus $T_{\text{eff}}(R_{\text{out}})$ for different \dot{M}, M_* parameters, with hollow symbols being scaled by 0.1x to naively demonstrate effects of the viewing angle. The self-gravitating disk naturally shows a “Hayashi limit”.

In this paper, we have focused primarily on modeling the dominant red/optical component of LRDs, but additional components in our scenario naturally explain the UV continuum emission of LRDs. Observationally, at least some LRDs are spatially resolved in the rest-frame UV (Chen et al. 2025a,b; Baggen et al. 2025), implying that at least part of the UV emission can be attributed to the host galaxy. This interpretation is also supported by spectroscopic decomposition results (Sun et al. 2026). Meanwhile, in our scenario, we expect the self-gravitating disk to give birth to a stellar population at a spatial scale comparable to the disk. The observed UV may come from the stars located in optically thin diffuse clouds that connects with the host galaxy at larger scales (see Figure 1). Our scenario is distinct from the standard AGN disk-related UV emission proposed by Zhang et al. (2025a), and we do not expect short-term UV variability from the stellar population. We note that the stellar mass function of this population can be extremely top-heavy due to the properties of initial fragment formation from gravitational instability and/or subsequent growth of stars from accretion in a gas-rich environment (Cantiello et al. 2021; Wang et al. 2023; Xu et al. 2025). Future work will aim to model the stellar populations in this environment in greater detail to make quantitative predictions for the UV appearance, guided by studies of stellar evolution in AGN disks.

The origin of the broad emission lines of LRDs remains a mystery. In our picture, UV radiation from stars at or larger than the disk scale powers the broad lines. The stellar ionizing spectrum is expected to be softer than that of a standard accretion disk, consistent with the weakness of high-ionization lines in at least some LRDs (Lambrides et al. 2024; Wang et al. 2025b). A stellar origin of the broad lines may also favor a lower UV-to-H α luminosity ratio than typical AGN, as recently measured for LRDs in Asada et al. (2026). The virial velocity at the disk scale can be estimated by (see Equation 16)

$$\sigma = \sqrt{\frac{GM_*}{R_{\text{out}}}} \approx 3 \times 10^2 \text{ km s}^{-1} \times \left(\frac{M_*}{10^6 M_\odot} \right)^{1/3} \left(\frac{\dot{M}/\alpha}{1 M_\odot \text{yr}^{-1}} \right)^{-1/9} \left(\frac{T_{\text{eff}}}{4000 \text{ K}} \right)^{3/8}. \quad (22)$$

This will be an upper limit if the UV-emitting regions are mainly located outside the optically thick region of the disk, where $R > R_{\text{out}}$. At low M_* , this estimate is insufficient to account for the observed line widths, although stellar potential may introduce additional velocity dispersion. Also, recent studies have suggested that scattering processes rather than virial motion are the main broadening mechanism (Rusakov et al. 2025; Naidu et al. 2025; Chang et al. 2025; Torralba et al. 2025; Sneppen et al. 2026; but see Juodžbalis et al. 2024;

Brazzini et al. 2025), in which case the intrinsic kinematic broadening will be less important. Furthermore, many LRDs show absorption features on top of the broad Balmer emission (Maiolino et al. 2025; Kocevski et al. 2024), indicative of a gas density $n > 10^8 \text{ cm}^{-3}$ (Juodžbalis et al. 2024), or $\rho > 10^{-16} \text{ g cm}^{-3}$. In our scenario, the characteristic gas density in the optically thin region of the disk is $\rho \lesssim 10^{-13} - 10^{-12} \text{ g cm}^{-3}$ (see Figure 3), so the broad line region can plausibly have the required gas density at the disk scale. Another possibility is that stellar-mass objects could generate H α through accretion shocks in optically thin environments, similar to H α generated by accretion of protostars (Lynden-Bell & Pringle 1974; Kurosawa et al. 2006) or protoplanets (Aoyama et al. 2018). Still, the exact location and geometry of the line-producing region remain uncertain, which we regard as an important topic for future investigation.

6.2. Metallicity and Dust Formation

Motivated by the non-detection of FIR emission in LRDs, we invoke dust-poor opacities in this study and show that they give rise to a universal outer effective temperature for optically thick, self-gravitating disk solutions (§2). For illustrative purposes, we employ zero-metallicity opacity tables in our numerical calculations, which leaves no dust-grain opacity below 2000K, only a very low molecular H₂ opacity floor. In this limit, any FIR-emitting optically thick disk solutions with $T_{\text{eff}} < 2000\text{K}$ (Thompson et al. 2005) is avoided for reasonable midplane ρ values relevant to our context (see Figure 2). While this represents an extreme dust-free case, the assumption can be relaxed in more general settings. In our framework, stellar evolution enriches the disk with metals as long as they are not completely dominated by an “immortal” population that continuously recycles gas with the environment (Jermyn et al. 2022), and metallicity evolution should therefore be incorporated into a time-dependent picture. Using MESA opacity tables with full grain opacity at non-negligible metallicity to produce Figure 9 as analogs of Figure 2, we find that dusty optically thick disk solutions emerge above critical midplane densities, with thresholds of e.g. $\rho \gtrsim 10^{-11}, 10^{-13}, 10^{-16} \text{ g cm}^{-3}$ at $[\text{M}/\text{H}] = 10^{-3}, 10^{-2}, 10^{-1}$ respectively. These thresholds may regulate the transition from LRD-like states to the classical appearance of dusty AGN, both over the lifetimes of individual systems and across cosmic time for the entire population. Concurrent with the growth of SMBH and evolution of stellar population, metal enrichment naturally leads to a decline of the abundance of LRD-like systems towards lower redshifts and higher luminosity (In-

ayoshi 2025; Ma et al. 2025b; Zhuang et al. 2025). Local LRD samples are found to have non-negligible metallicity and moderate mid-to-far-IR emission (Lin et al. 2025), qualitatively in agreement with this picture. The effect of metallicity evolution on FIR emission may also be generally relevant to observed nuclear color variations in JWST high-redshift quasars (Li et al. 2025).

Additional uncertainty arises from the possibility that, even at low temperatures, metals may remain predominantly in molecular form rather than condensing into dust grains (Lee et al. 2014), potentially due to inefficient nucleation (Johansen & Dorn 2022) or destruction processes (Rémy-Ruyer et al. 2014). In this scenario, the effective opacity can remain low even at non-negligible metallicities as molecular opacities are substantially weaker than grain opacities, subtly decoupling the broad notion of a “dust-poor” medium from that of a narrow “metal-poor” one. Exploring these possibilities and transitions in details will be an important direction for future work.

6.3. Cosmological Abundances

An important demographic constraint on the accretion properties of LRDs comes from the classical Soltan argument (Soltan 1982; Yu & Tremaine 2002), which relates the integrated luminosity output of growing black holes to the cumulative black-hole mass density in the local universe. Interpreted in this context, the mass density in SMBHs produced as putative LRD “relics” ρ_{LRD} is linked to the observed luminosity density of the population \mathcal{L}_{LRD} roughly by

$$\rho_{\text{LRD}} \sim \frac{\mathcal{L}_{\text{LRD}}}{c^2} \times \frac{\dot{M}_{\text{acc}}}{\dot{M}_{\text{lum}}} \times t_{\text{LRD}} \quad (23)$$

where t_{LRD} is the characteristic duration of the accretion phase (that can be observed), $\dot{M}_{\text{acc}}/\dot{M}_{\text{lum}}$ denotes the ratio between the total mass accreted and the mass converted into radiation, which is $(1 - \epsilon_{\bullet})/\epsilon_{\bullet} \sim 1/\epsilon_{\bullet}$ for accretion-powered source. Multi-band observations of LRDs have constrained their bolometric luminosities to be substantially lower than earlier estimates based on standard AGN bolometric corrections (Greene et al. 2025). With these recently revised luminosities, adopting a timescale of $t_{\text{LRD}} \sim 10^9 \text{ years}$ corresponding to the cosmic timescale at $z \sim 5$, and a canonical radiative efficiency $\epsilon_{\bullet} \sim 0.1$, the implied mass density $\rho_{\text{LRD}} \lesssim 10^4 - 10^5 M_{\odot} \text{Mpc}^{-3}$ for $\mathcal{L}_{\text{LRD}} \sim 10^{40} - 10^{41} \text{ erg s}^{-1} \text{Mpc}^{-3}$ would be below the local SMBH mass density $\rho_{\text{BH}} \sim 3 \times 10^5 M_{\odot} \text{Mpc}^{-3}$ estimated from other methods (e.g. Bernardi et al. 2010, 2013; Liepold & Ma 2024) and does not pose a significant Soltan-type tension. In fact, it would be consistent with the interpretation that

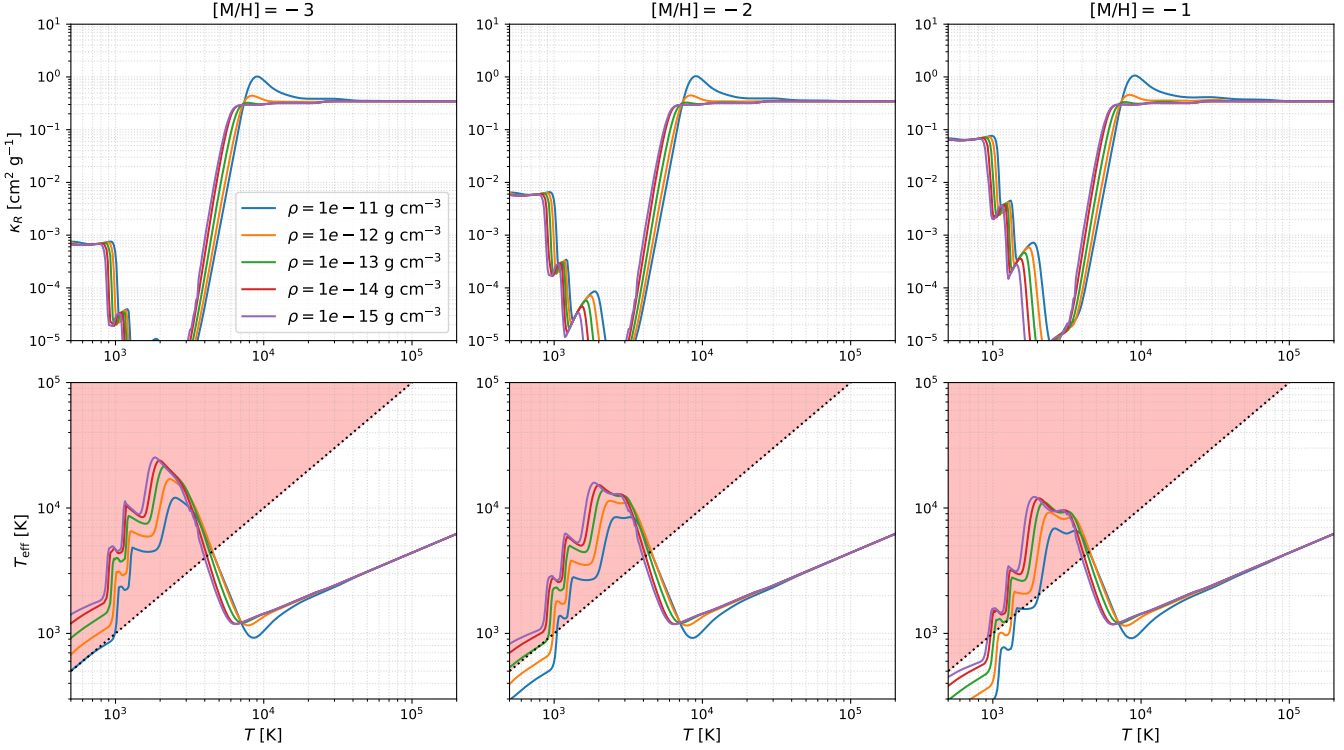


Figure 9. Similar to Figure 2 but for non-negligible $[M/H] = \log_{10} Z/Z_{\odot} = -3, -2, -1$, illustrating how dust grain opacity at higher metallicity progressively expands the region of parameter space that permits low temperature dusty optically thick disk solutions relevant to FIR emissions. Note that the opacities adopted here from Paxton (2024); Ferguson et al. (2005) include full grain opacity and do not account for the additional possibility that, even at low temperatures, metals may remain predominantly in molecular form, which would instead yield dust-poor opacities at non-negligible metallicity.

LRDs generally transition into AGNs around $z \sim 5$, a redshift below which their abundance undergoes a significant decline (Ma et al. 2025b; Umeda et al. 2025).

To assess whether a stellar-object-powered disk can satisfy the same demographic constraints, it is useful to note that the effective ratio between mass accreted and mass converted into luminosity is now

$$\frac{\dot{M}_{\text{acc}}}{\dot{M}_{\text{lum}}} \sim \frac{1}{\epsilon}, \quad (24)$$

which mainly depends on the characteristic radiative efficiency of stellar objects heating the self-gravitating disk (see §4). At the same time, \dot{M}_{acc} should be interpreted as the total mass inflow into the nuclear region. If all of the generated stellar mass eventually accrete onto the central black hole, e.g. by stellar tidal disruption and engulfment associated with extreme nuclear transients (Graham et al. 2025; Hinkle et al. 2025), the observed local SMBH mass density would impose a lower bound of $\epsilon \gtrsim 10^{-2}$ for LRDs. This would disfavor disk heating dominated by a conventional stellar population (Thompson et al. 2005) with $\epsilon \lesssim 10^{-3}$, and instead suggest that massive stars and/or stellar-

mass black holes provide the dominant heating source in our scenario. An alternative possibility is that a substantial fraction of the stellar mass formed in the self-gravitating region subsequently migrates outward or is ejected into the host galaxy, in which case the effective contribution to SMBH growth is reduced by a factor of $\sim \dot{M}(R_{\text{sg}})/\dot{M}(R_{\text{out}})$ from Equation 24, loosening the constraint or even quenching SMBH growth (Li et al. 2025). A more quantitative, redshift-dependent assessment of the allowed ranges of $\dot{M}(R_{\text{sg}})/\dot{M}(R_{\text{out}})$ and ϵ , as well as the properties and fate of the embedded (and potentially ejected) nuclear stellar population, will be explored in future studies.

6.4. Stellar Evolution in Quasar Disks

Finally, we comment that our model naturally appeals to more detailed studies of stellar evolution in AGN disks (Cantiello et al. 2021; Dittmann et al. 2021; Wang et al. 2021; Ali-Dib & Lin 2023; Chen et al. 2023a; Wang et al. 2023; Fan et al. 2024; Liu et al. 2024; Chen & Lin 2024; Xu et al. 2025), a line of work that has largely developed independently of galactic-scale star formation studies. In particular, complicated local processes like fragmentation, accretion, stellar winds, and

compositional mixing in AGN stars determine their initial and equilibrium mass functions, which in turn directly regulate both the effective radiative efficiency ϵ and the prominence of a UV continuum from stellar emission. A self-consistent treatment of the thermal equilibrium of massive star-heated, self-gravitating disks will ultimately require a new generation of radiation-hydrodynamic simulations, analogous in spirit to simulations of star formation and feedback on galactic scales (e.g. [Kim & Ostriker 2017](#)), but incorporating sink-particle prescriptions tailored to the unique properties of AGN stars and informed by detailed studies of local stellar evolution physics ([Chen et al. 2024, 2025c](#)). To capture spectral diagnostics such as line emission and

Balmer features, radiative transfer calculations may also need to move beyond the gray approximation toward multi-group treatments that resolve the multi-frequency vertical transport of radiation from the disk midplane to the photosphere. These directions represent natural extensions of the existing literature on stellar evolution and feedback in AGN disks and provide a pathway toward more predictive, observation-related studies of the appearance of stellar population in quasar disks.

ACKNOWLEDGEMENTS

Y.-X. C. thanks Douglas Lin, Liang Dai, Eugene Chiang, Chung-Pei Ma, Anna de Graaff and Minghao Guo for helpful discussions.

APPENDIX

A. GENERAL ρ, T, T_{EFF} SOLUTIONS FOR A RADIATION PRESSURE DOMINATED, SELF-GRAVITATING DISK

Given the disk equations in §2 and §3, the density and temperature profiles in a radiation pressure dominated $Q = 1$ disk with power law accretion rate profile $\dot{M} \propto R^\gamma$ has the following power law solution

$$\rho = \rho_0 (R/R_{\text{out}})^{-3}, T = T_0 (R/R_{\text{out}})^{-3/4+\gamma/6} \quad (\text{A1})$$

where the normalizations are

$$\rho_0 = \frac{M_\bullet}{2\pi R_{\text{out}}^3}, T_0 = \left[\frac{G\dot{M}_{\text{out}}}{\alpha} \left(\frac{3}{2\pi a} \right)^{3/2} \right]^{1/6} M_\bullet^{1/4} R_{\text{out}}^{-3/4} \quad (\text{A2})$$

setting $\kappa = \kappa(\rho_0, T_0)(\rho/\rho_0)^p(T/T_0)^q$,

$$T_{\text{eff}} = T_{\text{eff},0} (R/R_{\text{out}})^\eta, \eta = \left(-\frac{3}{16} + \frac{\gamma}{24} \right) (2 - q) + \frac{3p}{4} \quad (\text{A3})$$

where

$$T_{\text{eff},0} = \left[\frac{T_0^2}{\kappa_R(\rho_0, T_0) \sqrt{\frac{a}{6\pi G}}} \right]^{1/4} \quad (\text{A4})$$

In summary, the effective temperature profile of a radiation-pressure-dominated, self-gravitating disk is insensitive to the detailed accretion-rate radial dependence encoded by γ , which enters only weakly into the power-law index of $T_{\text{eff}}(R)$. For constant opacity ($p = q = 0$), we obtain $\partial \ln T_{\text{eff}} / \partial \ln R \simeq -3/8$ ([Sirk & Goodman 2003](#)), which is already significantly flatter than the canonical $-3/4$ scaling of a standard thin disk. We note that $\partial \ln T_{\text{eff}} / \partial \ln R > -1/2$ implies that the outer edge starts to dominate the total radiative output. Adopting a Kramers opacity ($p = 1, q = -3.5$) further flattens the profile to $\partial \ln T_{\text{eff}} / \partial \ln R \gtrsim -0.3$, albeit still declining. In contrast, when the opacity is dominated by H^- with $q \sim 9$, the resulting slope becomes positive, leading to an inverted effective temperature profile. In all cases, these scalings imply that self-gravitating disks generically have SEDs dominated by emission from their outer radii. The final case, corresponding to the H^- opacity, is particularly relevant for our numerical models, which predominantly reside in this regime near R_{out} .

REFERENCES

Akins, H. B., Casey, C. M., Lambrides, E., et al. 2025, *ApJ*, 991, 37, doi: [10.3847/1538-4357/ade984](https://doi.org/10.3847/1538-4357/ade984)
 Ali-Dib, M., & Lin, D. N. C. 2023, *MNRAS*, doi: [10.1093/mnras/stad2774](https://doi.org/10.1093/mnras/stad2774)

Aoyama, Y., Ikoma, M., & Tanigawa, T. 2018, The Astrophysical Journal, 866, 84, doi: [10.3847/1538-4357/aadc11](https://doi.org/10.3847/1538-4357/aadc11)

Asada, Y., Inayoshi, K., Fei, Q., Fujimoto, S., & Willott, C. 2026, arXiv e-prints, arXiv:2601.10573, doi: [10.48550/arXiv.2601.10573](https://doi.org/10.48550/arXiv.2601.10573)

Baggen, J. F. W., van Dokkum, P., Labb  , I., & Brammer, G. 2025, arXiv e-prints, arXiv:2512.03239, doi: [10.48550/arXiv.2512.03239](https://doi.org/10.48550/arXiv.2512.03239)

Begelman, M. C., & Dexter, J. 2025, arXiv e-prints, arXiv:2507.09085, doi: [10.48550/arXiv.2507.09085](https://doi.org/10.48550/arXiv.2507.09085)

Bernardi, M., Meert, A., Sheth, R. K., et al. 2013, MNRAS, 436, 697, doi: [10.1093/mnras/stt1607](https://doi.org/10.1093/mnras/stt1607)

Bernardi, M., Shankar, F., Hyde, J. B., et al. 2010, MNRAS, 404, 2087, doi: [10.1111/j.1365-2966.2010.16425.x](https://doi.org/10.1111/j.1365-2966.2010.16425.x)

Brazzini, M., D'Eugenio, F., Maiolino, R., et al. 2025, MNRAS, 544, L167, doi: [10.1093/mnrasl/slafl116](https://doi.org/10.1093/mnrasl/slafl116)

Burke, C. J., Stone, Z., Shen, Y., & Jiang, Y.-F. 2025, arXiv e-prints, arXiv:2511.16082, doi: [10.48550/arXiv.2511.16082](https://doi.org/10.48550/arXiv.2511.16082)

Cantiello, M., Jermyn, A. S., & Lin, D. N. C. 2021, ApJ, 910, 94, doi: [10.3847/1538-4357/abdf4f](https://doi.org/10.3847/1538-4357/abdf4f)

Casey, C. M., Akins, H. B., Finkelstein, S. L., et al. 2025, ApJL, 990, L61, doi: [10.3847/2041-8213/adfa91](https://doi.org/10.3847/2041-8213/adfa91)

Chang, S.-J., Gronke, M., Matthee, J., & Mason, C. 2025, MNRAS, doi: [10.1093/mnras/staf2131](https://doi.org/10.1093/mnras/staf2131)

Chen, C.-H., Ho, L. C., Li, R., & Inayoshi, K. 2025a, ApJL, 989, L12, doi: [10.3847/2041-8213/adee0a](https://doi.org/10.3847/2041-8213/adee0a)

Chen, C.-H., Ho, L. C., Li, R., & Zhuang, M.-Y. 2025b, ApJ, 983, 60, doi: [10.3847/1538-4357/ada93a](https://doi.org/10.3847/1538-4357/ada93a)

Chen, K., Ren, J., & Dai, Z.-G. 2023a, ApJ, 948, 136, doi: [10.3847/1538-4357/acc45f](https://doi.org/10.3847/1538-4357/acc45f)

Chen, Y.-X., Jiang, Y.-F., & Goodman, J. 2025c, ApJ, 987, 188, doi: [10.3847/1538-4357/addd0a](https://doi.org/10.3847/1538-4357/addd0a)

Chen, Y.-X., Jiang, Y.-F., Goodman, J., & Lin, D. N. C. 2024, ApJ, 974, 106, doi: [10.3847/1538-4357/ad6dd4](https://doi.org/10.3847/1538-4357/ad6dd4)

Chen, Y.-X., Jiang, Y.-F., Goodman, J., & Ostriker, E. C. 2023b, ApJ, 948, 120, doi: [10.3847/1538-4357/acc023](https://doi.org/10.3847/1538-4357/acc023)

Chen, Y.-X., & Lin, D. N. C. 2024, ApJ, 967, 88, doi: [10.3847/1538-4357/ad3c3a](https://doi.org/10.3847/1538-4357/ad3c3a)

de Graaff, A., Hviding, R. E., Naidu, R. P., et al. 2025a, arXiv e-prints, arXiv:2511.21820, doi: [10.48550/arXiv.2511.21820](https://doi.org/10.48550/arXiv.2511.21820)

de Graaff, A., Rix, Hans-Walter, Naidu, Rohan P., et al. 2025b, A&A, 701, A168, doi: [10.1051/0004-6361/202554681](https://doi.org/10.1051/0004-6361/202554681)

Dittmann, A. J., Cantiello, M., & Jermyn, A. S. 2021, ApJ, 916, 48, doi: [10.3847/1538-4357/ac042c](https://doi.org/10.3847/1538-4357/ac042c)

Epstein-Martin, M., Tagawa, H., Haiman, Z., & Perna, R. 2025, MNRAS, 537, 3396, doi: [10.1093/mnras/staf237](https://doi.org/10.1093/mnras/staf237)

Fan, X., Wu, Q., Wu, J., et al. 2024, ApJ, 966, 222, doi: [10.3847/1538-4357/ad395d](https://doi.org/10.3847/1538-4357/ad395d)

Ferguson, J. W., Alexander, D. R., Allard, F., et al. 2005, ApJ, 623, 585, doi: [10.1086/428642](https://doi.org/10.1086/428642)

Fu, S., Zhang, Z., Jiang, D., et al. 2025, arXiv e-prints, arXiv:2512.02096, doi: [10.48550/arXiv.2512.02096](https://doi.org/10.48550/arXiv.2512.02096)

Furtak, L. J., Secunda, A. R., Greene, J. E., et al. 2025, A&A, 698, A227, doi: [10.1051/0004-6361/202554110](https://doi.org/10.1051/0004-6361/202554110)

Gilbaum, S., & Stone, N. C. 2022, ApJ, 928, 191, doi: [10.3847/1538-4357/ac4ded](https://doi.org/10.3847/1538-4357/ac4ded)

Goodman, J. 2003, MNRAS, 339, 937, doi: [10.1046/j.1365-8711.2003.06241.x](https://doi.org/10.1046/j.1365-8711.2003.06241.x)

Goodman, J., & Rafikov, R. R. 2001, ApJ, 552, 793, doi: [10.1086/320572](https://doi.org/10.1086/320572)

Goodman, J., & Tan, J. C. 2004, ApJ, 608, 108, doi: [10.1086/386360](https://doi.org/10.1086/386360)

Graham, M. J., McKernan, B., Ford, K. E. S., et al. 2025, Nature Astronomy, doi: [10.1038/s41550-025-02699-0](https://doi.org/10.1038/s41550-025-02699-0)

Greene, J. E., Labbe, I., Goulding, A. D., et al. 2024, ApJ, 964, 39, doi: [10.3847/1538-4357/ad1e5f](https://doi.org/10.3847/1538-4357/ad1e5f)

Greene, J. E., Setton, D. J., Furtak, L. J., et al. 2025, arXiv e-prints, arXiv:2509.05434, doi: [10.48550/arXiv.2509.05434](https://doi.org/10.48550/arXiv.2509.05434)

Hinkle, J. T., Shappee, B. J., Auchettl, K., et al. 2025, Science Advances, 11, ead0074, doi: [10.1126/sciadv.adt0074](https://doi.org/10.1126/sciadv.adt0074)

Hopkins, P. F., & Quataert, E. 2010, MNRAS, 407, 1529, doi: [10.1111/j.1365-2966.2010.17064.x](https://doi.org/10.1111/j.1365-2966.2010.17064.x)

Hviding, R. E., de Graaff, A., Miller, T. B., et al. 2025, A&A, 702, A57, doi: [10.1051/0004-6361/202555816](https://doi.org/10.1051/0004-6361/202555816)

Iglesias, C. A., & Rogers, F. J. 1993, ApJ, 412, 752, doi: [10.1086/172958](https://doi.org/10.1086/172958)

—. 1996, ApJ, 464, 943, doi: [10.1086/177381](https://doi.org/10.1086/177381)

Inayoshi, K. 2025, ApJL, 988, L22, doi: [10.3847/2041-8213/adea66](https://doi.org/10.3847/2041-8213/adea66)

Inayoshi, K., & Maiolino, R. 2025, ApJL, 980, L27, doi: [10.3847/2041-8213/adaebd](https://doi.org/10.3847/2041-8213/adaebd)

Inayoshi, K., Shangguan, J., Chen, X., Ho, L. C., & Haiman, Z. 2025, arXiv e-prints, arXiv:2505.05322, doi: [10.48550/arXiv.2505.05322](https://doi.org/10.48550/arXiv.2505.05322)

Jermyn, A. S., Dittmann, A. J., McKernan, B., Ford, K. E. S., & Cantiello, M. 2022, ApJ, 929, 133, doi: [10.3847/1538-4357/ac5d40](https://doi.org/10.3847/1538-4357/ac5d40)

Ji, X., Maiolino, R.,   bler, H., et al. 2025, MNRAS, 544, 3900, doi: [10.1093/mnras/staf1867](https://doi.org/10.1093/mnras/staf1867)

Jiang, Y.-F., & Goodman, J. 2011, ApJ, 730, 45, doi: [10.1088/0004-637X/730/1/45](https://doi.org/10.1088/0004-637X/730/1/45)

Johansen, A., & Dorn, C. 2022, A&A, 662, A19, doi: [10.1051/0004-6361/202243480](https://doi.org/10.1051/0004-6361/202243480)

Juodžbalis, I., Ji, X., Maiolino, R., et al. 2024, MNRAS, 535, 853, doi: [10.1093/mnras/stae2367](https://doi.org/10.1093/mnras/stae2367)

Kido, D., Ioka, K., Hotokezaka, K., Inayoshi, K., & Irwin, C. M. 2025, MNRAS, 544, 3407, doi: [10.1093/mnras/staf1898](https://doi.org/10.1093/mnras/staf1898)

Kim, C.-G., & Ostriker, E. C. 2017, ApJ, 846, 133, doi: [10.3847/1538-4357/aa8599](https://doi.org/10.3847/1538-4357/aa8599)

Kocevski, D. D., Finkelstein, S. L., Barro, G., et al. 2024, arXiv e-prints, arXiv:2404.03576, doi: [10.48550/arXiv.2404.03576](https://doi.org/10.48550/arXiv.2404.03576)

Kokorev, V., Caputi, K. I., Greene, J. E., et al. 2024, ApJ, 968, 38, doi: [10.3847/1538-4357/ad4265](https://doi.org/10.3847/1538-4357/ad4265)

Kurosawa, R., Harries, T. J., & Symington, N. H. 2006, Monthly Notices of the Royal Astronomical Society, 370, 580596, doi: [10.1111/j.1365-2966.2006.10527.x](https://doi.org/10.1111/j.1365-2966.2006.10527.x)

Labbé, I., van Dokkum, P., Nelson, E., et al. 2023, Nature, 616, 266, doi: [10.1038/s41586-023-05786-2](https://doi.org/10.1038/s41586-023-05786-2)

Labbe, I., Greene, J. E., Matthee, J., et al. 2024, arXiv e-prints, arXiv:2412.04557, doi: [10.48550/arXiv.2412.04557](https://doi.org/10.48550/arXiv.2412.04557)

Lambrides, E., Garofali, K., Larson, R., et al. 2024, arXiv e-prints, arXiv:2409.13047, doi: [10.48550/arXiv.2409.13047](https://doi.org/10.48550/arXiv.2409.13047)

Lee, E. J., Chiang, E., & Ormel, C. W. 2014, ApJ, 797, 95, doi: [10.1088/0004-637X/797/2/95](https://doi.org/10.1088/0004-637X/797/2/95)

Li, R., Ho, L. C., & Chen, C.-H. 2025, arXiv e-prints, arXiv:2505.12867, doi: [10.48550/arXiv.2505.12867](https://doi.org/10.48550/arXiv.2505.12867)

Liepold, E. R., & Ma, C.-P. 2024, ApJL, 971, L29, doi: [10.3847/2041-8213/ad66b8](https://doi.org/10.3847/2041-8213/ad66b8)

Lin, X., Wang, F., Fan, X., et al. 2024, ApJ, 974, 147, doi: [10.3847/1538-4357/ad6565](https://doi.org/10.3847/1538-4357/ad6565)

Lin, X., Fan, X., Cai, Z., et al. 2025, arXiv e-prints, arXiv:2507.10659, doi: [10.48550/arXiv.2507.10659](https://doi.org/10.48550/arXiv.2507.10659)

Liu, H., Jiang, Y.-F., Quataert, E., Greene, J. E., & Ma, Y. 2025, ApJ, 994, 113, doi: [10.3847/1538-4357/ae0c19](https://doi.org/10.3847/1538-4357/ae0c19)

Liu, J.-R., Wang, Y.-L., & Wang, J.-M. 2024, ApJ, 969, 37, doi: [10.3847/1538-4357/ad463a](https://doi.org/10.3847/1538-4357/ad463a)

Lynden-Bell, D., & Pringle, J. E. 1974, MNRAS, 168, 603, doi: [10.1093/mnras/168.3.603](https://doi.org/10.1093/mnras/168.3.603)

Ma, Y., Greene, J. E., Setton, D. J., et al. 2025a, ApJ, 981, 191, doi: [10.3847/1538-4357/ada613](https://doi.org/10.3847/1538-4357/ada613)

—. 2025b, arXiv e-prints, arXiv:2504.08032, doi: [10.48550/arXiv.2504.08032](https://doi.org/10.48550/arXiv.2504.08032)

Maiolino, R., Risaliti, G., Signorini, M., et al. 2025, MNRAS, 538, 1921, doi: [10.1093/mnras/staf359](https://doi.org/10.1093/mnras/staf359)

Matthee, J., Naidu, R. P., Brammer, G., et al. 2024, ApJ, 963, 129, doi: [10.3847/1538-4357/ad2345](https://doi.org/10.3847/1538-4357/ad2345)

Naidu, R. P., Matthee, J., Katz, H., et al. 2025, arXiv e-prints, arXiv:2503.16596, doi: [10.48550/arXiv.2503.16596](https://doi.org/10.48550/arXiv.2503.16596)

Nandal, D., & Loeb, A. 2025, arXiv e-prints, arXiv:2507.12618, doi: [10.48550/arXiv.2507.12618](https://doi.org/10.48550/arXiv.2507.12618)

Paxton, B. 2024, Modules for Experiments in Stellar Astrophysics (MESA), r24.08.1, Zenodo, doi: [10.5281/zenodo.13353788](https://doi.org/10.5281/zenodo.13353788)

Rémy-Ruyer, A., Madden, S. C., Galliano, F., et al. 2014, A&A, 563, A31, doi: [10.1051/0004-6361/201322803](https://doi.org/10.1051/0004-6361/201322803)

Rozyczka, M., Bodenheimer, P., & Lin, D. N. C. 1995, MNRAS, 276, 597, doi: [10.1093/mnras/276.2.597](https://doi.org/10.1093/mnras/276.2.597)

Rusakov, V., Watson, D., Nikopoulos, G. P., et al. 2025, arXiv e-prints, arXiv:2503.16595, doi: [10.48550/arXiv.2503.16595](https://doi.org/10.48550/arXiv.2503.16595)

Setton, D. J., Greene, J. E., Spilker, J. S., et al. 2025, ApJL, 991, L10, doi: [10.3847/2041-8213/ade78b](https://doi.org/10.3847/2041-8213/ade78b)

Shakura, N. I., & Sunyaev, R. A. 1973, A&A, 24, 337

Sirko, E., & Goodman, J. 2003, MNRAS, 341, 501, doi: [10.1046/j.1365-8711.2003.06431.x](https://doi.org/10.1046/j.1365-8711.2003.06431.x)

Sneppen, A., Watson, D., Matthews, J. H., et al. 2026, arXiv e-prints, arXiv:2601.18864, doi: [10.48550/arXiv.2601.18864](https://doi.org/10.48550/arXiv.2601.18864)

Soltan, A. 1982, MNRAS, 200, 115, doi: [10.1093/mnras/200.1.115](https://doi.org/10.1093/mnras/200.1.115)

Sun, W. Q., Naidu, R. P., Matthee, J., et al. 2026, arXiv e-prints, arXiv:2601.20929, <https://arxiv.org/abs/2601.20929>

Tagawa, H., Haiman, Z., & Kocsis, B. 2020, ApJ, 898, 25, doi: [10.3847/1538-4357/ab9b8c](https://doi.org/10.3847/1538-4357/ab9b8c)

Thompson, T. A., Quataert, E., & Murray, N. 2005, ApJ, 630, 167, doi: [10.1086/431923](https://doi.org/10.1086/431923)

Torralba, A., Matthee, J., Pezzulli, G., et al. 2025, arXiv e-prints, arXiv:2510.00103, doi: [10.48550/arXiv.2510.00103](https://doi.org/10.48550/arXiv.2510.00103)

Umeda, H., Inayoshi, K., Harikane, Y., & Murase, K. 2025, arXiv e-prints, arXiv:2512.04208, doi: [10.48550/arXiv.2512.04208](https://doi.org/10.48550/arXiv.2512.04208)

Wang, B., Leja, J., de Graaff, A., et al. 2024, ApJL, 969, L13, doi: [10.3847/2041-8213/ad55f7](https://doi.org/10.3847/2041-8213/ad55f7)

Wang, B., de Graaff, A., Davies, R. L., et al. 2025a, ApJ, 984, 121, doi: [10.3847/1538-4357/adc1ca](https://doi.org/10.3847/1538-4357/adc1ca)

Wang, B., Leja, J., Katz, H., et al. 2025b, arXiv e-prints, arXiv:2508.18358, doi: [10.48550/arXiv.2508.18358](https://doi.org/10.48550/arXiv.2508.18358)

Wang, B., Leja, J., Labbe, I., et al. 2026, arXiv e-prints, arXiv:2602.06024, <https://arxiv.org/abs/2602.06024>

Wang, J.-M., Liu, J.-R., Ho, L. C., Li, Y.-R., & Du, P. 2021, ApJL, 916, L17, doi: [10.3847/2041-8213/ac0b46](https://doi.org/10.3847/2041-8213/ac0b46)

Wang, J.-M., Zhai, S., Li, Y.-R., et al. 2023, ApJ, 954, 84, doi: [10.3847/1538-4357/acdf48](https://doi.org/10.3847/1538-4357/acdf48)

Wang, J.-M., Wang, Y.-L., Chen, Y.-J., et al. 2025c, arXiv e-prints, arXiv:2511.09278, doi: [10.48550/arXiv.2511.09278](https://doi.org/10.48550/arXiv.2511.09278)

Williams, C. C., Alberts, S., Ji, Z., et al. 2024, ApJ, 968, 34, doi: [10.3847/1538-4357/ad3f17](https://doi.org/10.3847/1538-4357/ad3f17)

Xiao, M., Oesch, P. A., Bing, L., et al. 2025, A&A, 700, A231, doi: [10.1051/0004-6361/202554361](https://doi.org/10.1051/0004-6361/202554361)

Xu, Z.-H., Chen, Y.-X., & Lin, D. N. C. 2025, arXiv e-prints, arXiv:2511.03904, doi: [10.48550/arXiv.2511.03904](https://doi.org/10.48550/arXiv.2511.03904)

Yu, Q., & Tremaine, S. 2002, MNRAS, 335, 965, doi: [10.1046/j.1365-8711.2002.05532.x](https://doi.org/10.1046/j.1365-8711.2002.05532.x)

Zhang, C., Wu, Q., Fan, X., et al. 2025a, arXiv e-prints, arXiv:2505.12719, doi: [10.48550/arXiv.2505.12719](https://doi.org/10.48550/arXiv.2505.12719)

Zhang, Z., Jiang, L., Liu, W., & Ho, L. C. 2025b, ApJ, 985, 119, doi: [10.3847/1538-4357/adcb3e](https://doi.org/10.3847/1538-4357/adcb3e)

Zhang, Z., Li, M., Oguri, M., et al. 2025c, arXiv e-prints, arXiv:2512.05180. <https://arxiv.org/abs/2512.05180>

Zhou, S., Sun, M., Liu, T., et al. 2024, ApJL, 966, L9, doi: [10.3847/2041-8213/ad3c3f](https://doi.org/10.3847/2041-8213/ad3c3f)

Zhuang, M.-Y., Li, J., Shen, Y., et al. 2025, arXiv e-prints, arXiv:2505.20393, doi: [10.48550/arXiv.2505.20393](https://doi.org/10.48550/arXiv.2505.20393)

Zwick, L., Tiede, C., & Mayer, L. 2025, arXiv e-prints, arXiv:2507.22014, doi: [10.48550/arXiv.2507.22014](https://doi.org/10.48550/arXiv.2507.22014)